The Efficacy of the Mean Filter on the Noise Reduction of Digitalized Images

Chowdappa Manne Ramanna
Department of Mathematics, SJC Institute of Technology, Chickballapur-562101, Karnataka, India
chowdappamr.maths@sjcit.ac.in

Udaya Kumara Kodipalya Nanjappa
Department of Mathematics, School of Applied Sciences, REVA University, Bengaluru, Karnataka, India
udayakumarkn@reva.edu.in

Sreenivasa Reddy Perla
Department of Mathematics, SJC Institute of Technology, Chickballapur-562101, Karnataka, India
srireddy_sri@yahoo.co.in

Nagaraja Kurugal Munikempanna
Department of Mathematics, JSS Academy of Technical Education, Uttarahalli-Kengeri Main Road, Bengaluru-560 060, Karnataka, India
nagkmn@gmail.com (corresponding author)

Sampathkumar Ramachandraiah
Department of Mathematics, RNS Institute of Technology, Bengaluru, India
r.sampathkumar1967@gmail.com

Venkataramana B. Siddappa
Department of Mathematics, KS Institute of Technology, Bengaluru, India
venkynvs@gmail.com

Received: 5 March 2025 | Revised: 9 April 2025 | Accepted: 15 April 2025

 DOI: https://doi.org/10.48084/etasr.10809

ABSTRACT

Digital Image Processing (DIP) involves the use of a digital computer to process images, where noise introduced during transmission is reduced using suitable filters. Noise reduction is crucial as image quality directly affects result accuracy. This study explores various filters on common images with different types of noise. The Power Exponential Mean (PEM) filter shows strong correlation performance on the Hilbert-curve image with consistent parameters. The results indicate that PEM filters are robust, outperforming other spatial mean filters. PEM maintains performance even with changing image resolution, proving its reliability. It also preserves image structure, luminosity, and granularity, even at large kernel sizes. Many filters degrade at larger kernel sizes, but PEM retains image information. The quantitative evaluation utilized MSE, PSNR, CoC, and MAE, with MATLAB 14b for assessment.

Keywords-PSNR; MSE; CoC; MAE; noise; mean filters

I. INTRODUCTION

Image filtering plays an important role in image processing applications, such as medical imaging, computer vision, and digital photography. It enhances image quality by reducing noise, improving contrast, and preserving essential features. In medical imaging, filtering is especially important for reducing speckle noise that can obscure diagnostic details [1]. Authors in [2] presented an improved "de-noising" algorithm for removing noise in color images. Traditional filters, like mean and median, have been widely employed for noise reduction [3, 4], but often fall short in preserving edges and fine features. More advanced approaches, such as directional, hybrid, and classification-based filtering have shown superior performance in tasks, like skin cancer detection and medical image enhancement [5, 6]. Recent developments, including

mathematical models based on PEM and invariant properties, have further improved image filtering capabilities [7-9]. Emerging methods, like Iterative Window Mean Filtering (IWMF), also seem promising for adversarial purification and effective noise reduction [10]. Authors in [11] investigated an anisotropic diffusion adaptive filter for image de-noising and restoration, applied on satellite remote sensing images. Filter efficiency is commonly evaluated based on noise reduction, computational cost, and edge retention [12]. The present study reviews and compares these filtering techniques to identify the most effective approaches for specific image processing tasks.

A. *Mean Filters*

The various mean filter types used in the literature [13] for noise reduction are:

- Contra-harmonic-Mean filter:

$$\hat{f}(x,y)=\frac{\sum_{(s,t)\in s_{xy}} g(s,t)^{Q+1}}{\sum_{(s,t)\in s_{xy}} g(s,t)^{Q}} \quad (1)$$

where S_{xy} is the image window centered at (x,y), g is the input function, and Q is a real number parameter controlling the nature of the filter (Q-filter order). When Q=0, the filter is the arithmetic mean and when Q=-1, it is the harmonic mean. Also pepper-noise is reduced when Q takes positive values and the salt-noise is reduced when Q takes negative values.

- Harmonic-mean filter:

$$\hat{f}(x,y)=\frac{mn}{\sum_{(s,t)\in s_{xy}} \frac{1}{g(s,t)}} \quad (2)$$

where $m\times n$ is the size of the image.

- Centroidal-mean filter:

$$\hat{f}(x,y)=\frac{1}{3}\frac{mn}{\sum_{(s,t)\in s_{xy}} \frac{1}{g(s,t)}}+\frac{2}{3}\frac{\sum_{(s,t)\in s_{xy}} g(s,t)^{Q+1}}{\sum_{(s,t)\in s_{xy}} g(s,t)^{Q}} \quad (3)$$

- Heron-mean filter:

$$\hat{f}(x,y)=\frac{1}{mn}\sum_{(s,t)\in s_{xy}} g(s,t)+\left(\prod_{(s,t)\in s_{xy}} g(s,t)\right)^{\frac{1}{mn}} \quad (4)$$

- Inverse contra-harmonic-mean filter:

$$\hat{f}(x,y)=\left(\prod_{(s,t)\in s_{xy}} g(s,t)\right)^{\frac{1}{mn}} * \left(\frac{\sum_{(s,t)\in s_{xy}} g(s,t)^{Q+1}}{\sum_{(s,t)\in s_{xy}} g(s,t)^{Q}}\right) \quad (5)$$

Simulation analysis using MATLAB was conducted on an original camera image with four noise types: Poisson, Gaussian, Speckle, and Salt and Pepper [11]. Moreover, quantitative evaluation of de-noised images was carried out using PSNR, MSE, CoC, and MAE metrics. These parameters were measured for various filters: centroidal mean, contra harmonic mean, inverse contra harmonic mean, harmonic mean, and heron mean at different filter orders (Q = -2, -1, 1, 2). The quality of the filtered images was also assessed to compare performance across noise types. The results showed that the centroidal mean filter works very well for Salt and Pepper noise removal, the inverse contra harmonic mean filter works very well for Speckle noise removal, and the contra harmonic, harmonic, and heron mean filters work very well for Poisson noise removal.

Two more mean value filters are introduced in the present study [9]:

- Power-exponential mean:

$$\hat{f}(x,y)=\left(\prod_{(s,t)\in s_{xy}} g(s,t)\right)^{\frac{\alpha}{\sum_{(s,t)\in s_{xy}} g(s,t)^{\alpha}}} \quad (6)$$

where α is the power parameter that controls emphasis on pixel intensities.

- Invariant power-exponential mean:

$$\hat{f}(x,y)=\left[\left(\prod_{(s,t)\in s_{xy}} g(s,t)\right)^{\frac{\alpha}{\sum_{(s,t)\in s_{xy}} g(s,t)^{\alpha}}}\right]^{\frac{1}{\alpha}} \quad (7)$$

II. STEPS FOR IMAGE DE-NOISING

The steps involved in the image noise removal process can be summarized in the chart displayed in Figure 1.

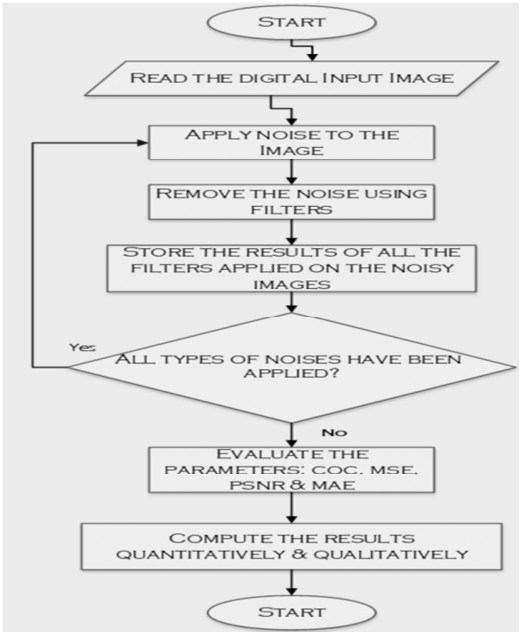

Fig. 1. Image de-noising.

III. STATISTICAL PARAMETERS

The statistical parameters studied in this paper are:

- Correlation of Coefficient r : is a statistical parameter used to measure the direction and strength of a linear relationship involving two variables. It takes values in the interval $[-1, 1]$ and it is calculated by:

$$r = \frac{\sum x_i y_i}{\sqrt{\sum x_i^2 \sum y_i^2}} \quad (8)$$

Positive or negative values of r denote, respectively, the positive or negative correlation between the variables x, y. In a positive correlation, both variables increase together. Correlation also depends on the PSNR of the images.

- Spectral Angle Mapper (SAM): It is a statistical method that works on image spectrum and returns the angular difference between the reference spectrum and the de-noised image. It is calculated in rad by:

$$\alpha = cos^{-1}\left(\frac{\sum xy}{\sqrt{\sum x^2 \sum y^2}}\right) \quad (9)$$

where x is the de-noised image and y is the reference image.

- Peak-Signal to Noise-Ratio (PSNR): It is an important parameter related to image quality. It is calculated by:

$$\text{PSNR} = 10\log_{10}\frac{R^2}{\sqrt{\text{MSE}}} \quad (10)$$

where R is the highest pixel value that appears in the image and MSE is the Mean Square Error between the de-noised and the original image, the size of which is $m \times n$.

- Visual-Information-Fidelity (VIF): It is a parameter used to assess the fidelity of a processed image compared to its original version. It quantifies the amount of visual information preserved during image processing or compression.

- Mean-Absolute-Error (MAE): It determines the difference among the predicted and observed values. It is calculated by:

$$\text{MAE} = \frac{1}{N}\sum_{I=1}^{N}\left|x_{pred} - x_{obs}\right| \quad (11)$$

where x_{pred}, x_{obs} are the predicted and observed values, respectively, and N is the number of observations.

IV. SIMULATION RESULTS

The analysis in the current paper aims to measure the influence of different filters on various noise types and images, to identify the most suitable ones for the reduction of different noise types, and to investigate the role of various image parameters. The Poisson, Salt and Pepper, Gaussian, and Speckle noise are corrupting the images. All four noise types are removed by the following types of filters: centroidal mean filter, contra-harmonic mean filter, inverse contra-harmonic-mean filter, harmonic mean filter, Heron mean filter, and invariant power-exponential mean and power-exponential mean filters. The open CV unit of Python is used to de-noise the image. Computational accelerations are utilized in filtering to run with better resolution and kernel sizes. Also, Just-In-Time (JIT) and GPU-compiler are deployed to boost calculation speed. The IPEM filter is combined with promising spatial-mean filters, which offer effective de-noising capabilities. Regarding image estimation involving normal images, statistical specificity and noise models are employed. Additionally, the typical Hilbert curve and Lena images are used (Figure 2).

(a)

(b)

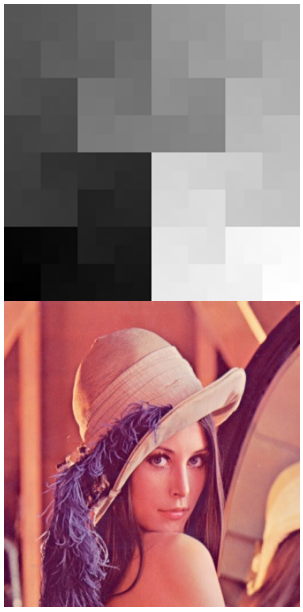

Fig. 2. (a) Hilbert curve image, (b) Lena image.

(a)

(b)

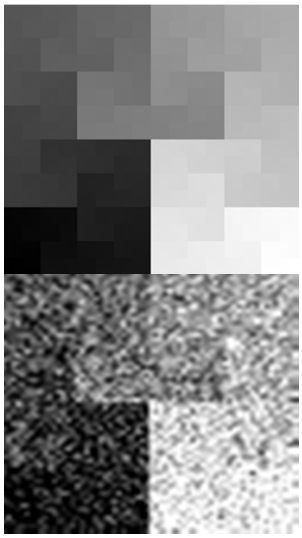

Fig. 3. Original, (b) 50% Gaussian noise.

Figure 3 is displays the original image and the one affected by 50% Gaussian noise. It is demonstrated that the PEM filters preserve the original image structure while introducing a slight blur, making it difficult for the affected image to relate to the original one.

(a)

(b)

(c)

(d)

(e)

(f)

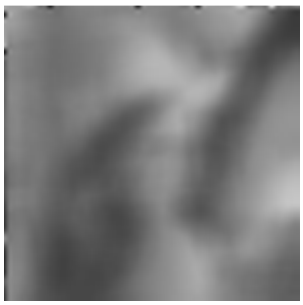

Fig. 4. Lena's image: (a) original; (b) 50% Salt and Pepper noise, (c) median 3 × 3, (d) median 9 × 9, (e) PEM 3 × 3, and (f) PEM 9 × 9.

Figure 4 presents Lena's original image alongside one corrupted with Salt and Pepper noise. With a 3×3 kernel size, the median filter can produce a relatively accurate image; though, the edges appear smudged. These images demonstrate that PEM performs better with larger kernel sizes compared to median filters. While median filter blurs the image excessively, making it hard to recognize the original details, PEM manages to blur the image while still preserving its original structure.

Figure 5 depicts the Lena's image in 64 × 64 resolution affected by Gaussian noise. PEM effectively preserves image details, providing superior filtering at such low resolutions.

(a)

(b)

Fig. 5. Lena's image: (a) original, (b) 50% Gaussian noise.

V. VARIOUS IMAGE RESOLUTIONS AND THEIR ANALYSIS

In order to conduct a thorough analysis of filtering techniques, the current study focuses on Gaussian and Salt and Pepper noises applied to Hilbert-curve and Lena's images. The filtering process involves assessing various statistical parameters to evaluate noise reduction effectiveness.

Comparing the (Tables I, II) filter value data under different MAE conditions in both images and then representing them with graphs (Figures 6, 7) helps in understanding the effectiveness of the filter settings at different resolutions and kernel sizes. Thus, insights into the optimal parameters for noise reduction in digital images are provided.

TABLE I. MAE: HILBERT CURVE IMAGE-GAUSSIAN NOISE.

MAE: Hilbert curve image						
Parameter	**Heron**	**Median**	**PEM**	**CMF**	**ICHM**	**IPEM**
Resolution 32 × 32 Kernel size 7 × 7	0.1080	0.1139	0.0786	0.1365	0.1612	0.1799
Resolution 64 × 64 Kernel size 7 × 7	0.0733	0.1025	0.0605	0.0949	0.1185	0.1185
Resolution 128 × 128 Kernel size 9 × 9	0.0587	0.0991	0.0515	0.0754	0.1037	0.0515
Resolution 256 × 256 Kernel size 9 × 9	0.0461	0.0957	0.0458	0.0554	0.0848	0.0458

From the result analysis, it is concluded that the resolution of 256 × 256 and Kernel size of 9 × 9 have lower MAE values, indicating the need for a better model or filtering process with fewer deviations from the actual values. Also the resolution 32 × 32 and Kernel size 7 × 7 has higher MAE suggesting significant deviations and lower accuracy.

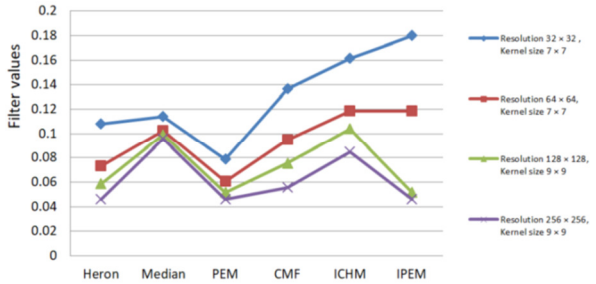

Fig. 6. MAE: Hilbert curve image-Gaussian noise filtering.

TABLE II. MAE: LENA'S IMAGE AND SALT AND PEPPER NOISE.

MAE: Lena's image						
Parameter	**Heron**	**Median**	**PEM**	**CMF**	**ICHM**	**IPEM**
Resolution 32 × 32 Kernel size 7 × 7	0.1084	0.1116	0.0992	0.1257	0.1600	0.0992
Resolution 64 × 64 Kernel size 7 × 7	0.0866	0.0752	0.0803	0.1062	0.1389	0.0803
Resolution 128 × 128 Kernel size 9 × 9	0.0746	0.0637	0.0681	0.0903	0.1245	0.0681
Resolution 256 × 256 Kernel size 9 × 9	0.0411	0.0503	0.0643	0.0624	0.1004	0.0643

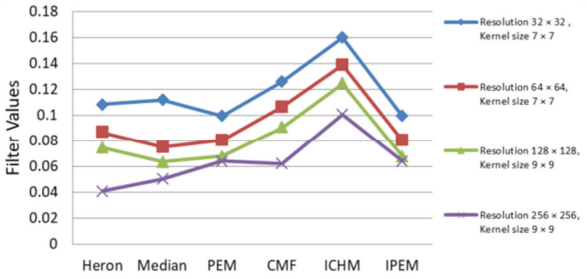

Fig. 7. MAE: Lena's image and Salt and Pepper noise filtering.

Studying the graph of VIF: Hilbert curve image and Gaussian noise (Figure 8), as well as the graph of VIF: Lena's image and Salt and Pepper noise (Figure 9), with filtering of various resolutions and varying Kernel sizes it is concluded that:

- When VIF = 1, the distorted image retains all visual information of the original image (perfect quality).
- When VIF < 1, the distorted image has lost some visual information (degraded quality).
- When VIF ≈ 0, the image contains almost no useful information from the original one (severe degradation).

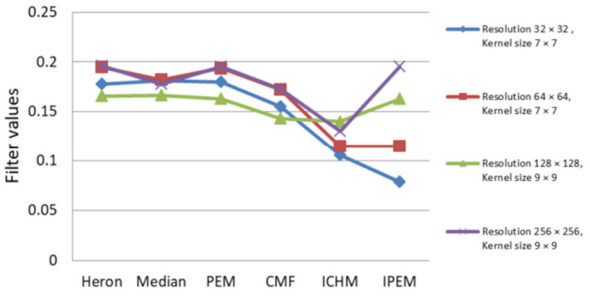

Fig. 8. VIF: Hilbert curve image andGaussian noise filtering.

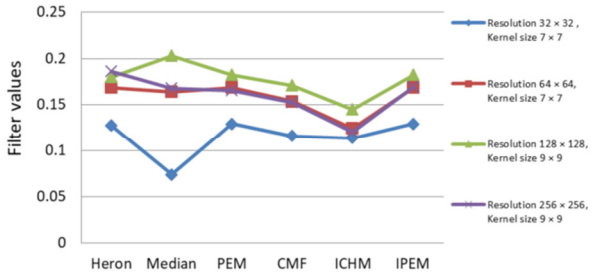

Fig. 9. VIF: Lena's image and Salt and Pepper noise filtering.

Observing the graph of SAM: Hilbert curve image and Gaussian noise (Figure 10) and the graph of the SAM: Lena's image and Salt and Pepper noise (Figure 11), with filtering of various resolutions and varying Kernel sizes, the conclusions drawn are:

- When SAM = 0°, the spectrum perfectly matches the reference spectrum.
- When SAM < 5°, the high spectral similarity indicates minimal distortion.
- When SAM > 10°, the significant spectral distortion suggests data corruption or improper processing.

SAM values are typically expressed in degrees or radians, with lower values indicating better spectral fidelity.

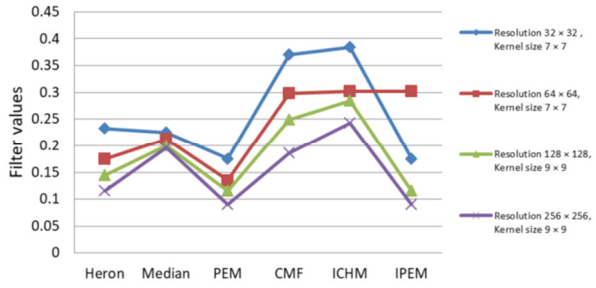

Fig. 10. SAM: Hilbert curve image and Gaussian noise filtering.

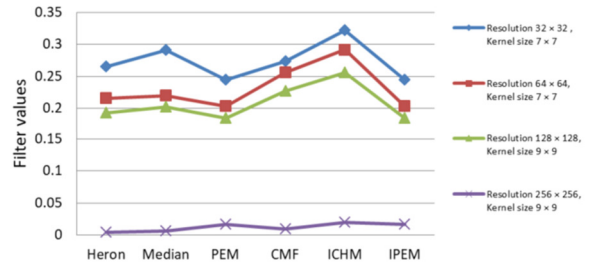

Fig. 11. SAM: Lena's image and Salt and Pepper noise filtering.

Studying the graphs of CoC: Hilbert curve image and Gaussian noise (Figure 12) and CoC: Lena's image and Salt and Pepper noise (Figure 13, with filtering of various resolutions and varying Kernel sizes, it is concluded that:

- When CoC ≈ 1, a strong similarity between the original and processed images is displayed, meaning minimal distortion.
- When 0.5 < CoC < 0.9, the processed image retains some but not all original features, suggesting partial similarity.
- When CoC ≈ 0, there is a significant loss of information due to noise, compression, or filtering, implying weak correlation.
- When CoC < 0, the image features are significantly altered or inverted, suggesting that the processed image is negatively correlated with the original one.

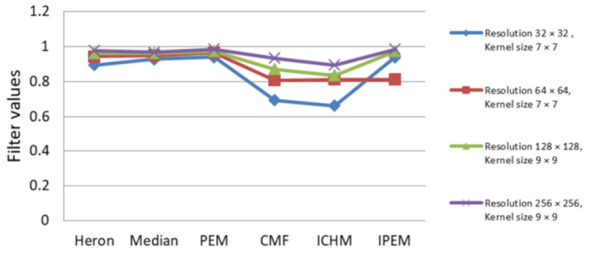

Fig. 12. CoC: Hilbert curve image and Gaussian noise filtering.

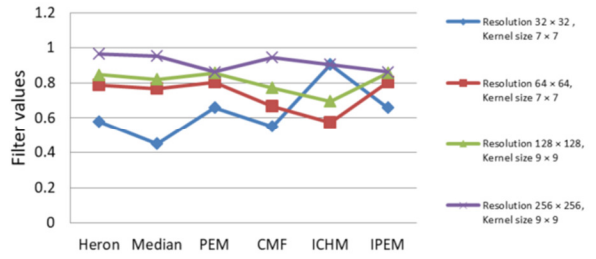

Fig. 13. CoC: Lena's image and Salt and Pepper noise filtering.

Observing the graph of PSNR: Hilbert curve image and Gaussian noise (Figure 14) and the graph of the PSNR: Lena's image and Salt and Pepper noise (Figure 15), with filtering of various resolutions and varying Kernel sizes, the main conclusion is that higher PSNR gives better image quality, meaning that the edited image is closer to the original one.

Some typical PSNR ranges in relation to image quality are:

- PSNR > 40 dB gives excellent quality (almost indistinguishable from the original).
- 30 dB < PSNR < 40 dB gives good quality (minor distortion visible).
- 20 dB < PSNR < 30 dB gives acceptable quality (noticeable distortion).
- PSNR < 20 dB gives poor quality (significant distortion).

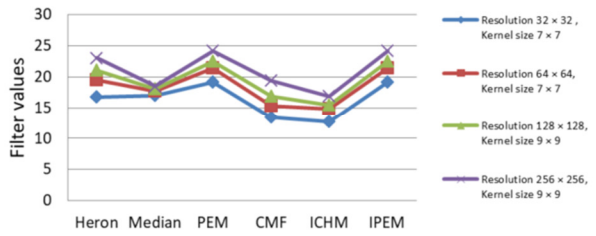

Fig. 14. PSNR: Hilbert curve image and Gaussian noise filtering.

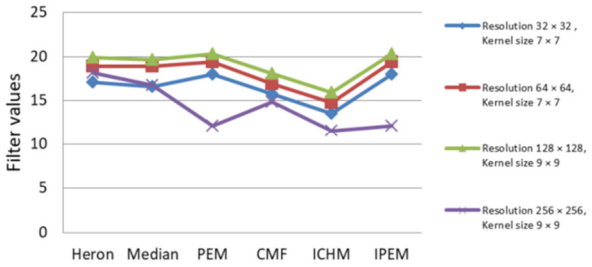

Fig. 15. PSNR: Lena's image and Salt and Pepper noise filtering.

VI. CONCLUSION

The Heron mean filter applied to an image with a resolution of 256 × 256 and a kernel size of 9 × 9 achieves a lower MAE value, indicating a highly effective filtering process with minimal deviation from the original image. Conversely, a 32 × 32 resolution with a 7 × 7 kernel size, results in a significantly higher MAE suggesting considerable deviations and reduced accuracy. This effect is particularly evident in Lena's image, where the 32 × 32 resolution and 7 × 7 kernel size further emphasize greater deviations and diminished filtering precision. Additionally, all mean filters exhibit degraded image quality when evaluated using the VIF metric.

However, the SAM metric indicates a perfect match for both Lena's image and the Hilbert-curve image when processed at a 256 × 256 resolution with a 9 × 9 kernel size.

In terms of CoC, the Heron mean filter at 256 × 256 resolution and 9 × 9 kernel size demonstrates strong correlation for Lena's image, while the Invariant Power Exponential Mean (PEM) filter with the same parameters achieves a good correlation for the Hilbert-curve image. When analyzed using PSNR, a 128 × 128 resolution with a 9 × 9 kernel size provides superior image quality for Lena's image, whereas a 256 × 256 resolution with the same kernel size leads to lower image quality.

In contrast, for the Hilbert-curve image, a 32 × 32 resolution with a 7 × 7 kernel size results in poor image quality, while a 256 × 256 resolution with a 9 × 9 kernel size significantly improves image quality, as reflected in PSNR measurements.

REFERENCES

[1] V. Bhateja, A. Srivastava, G. Singh, and J. Singh, "A Modified Speckle Suppression Algorithm for Breast Ultrasound Images Using Directional Filters," in *ICT and Critical Infrastructure: Proceedings of the 48th Annual Convention of Computer Society of India- Vol II*, Cham, 2014, pp. 219–226, https://doi.org/10.1007/978-3-319-03095-1_24.

[2] S. Rani, Y. Chabrra, and K. Malik, "An Improved Denoising Algorithm for Removing Noise in Color Images," *Engineering, Technology & Applied Science Research*, vol. 12, no. 3, pp. 8738–8744, Jun. 2022, https://doi.org/10.48084/etasr.4952.

[3] R. Chandel and G. Gupta, "Image Filtering Algorithms and Techniques: A Review," *International Journal of Advanced Research in Computer Science and Software Engineering*, vol. 3, no. 10, pp. 198–202, Oct. 2013.

[4] M. Sun, "Comparison of processing results of median filter and mean filter on Gaussian noise," *Applied and Computational Engineering*, vol. 5, pp. 779–785, May 2023, https://doi.org/10.54254/2755-2721/5/20230702.

[5] A. N. Hoshyar, A. Al-Jumaily, and A. N. Hoshyar, "Comparing the Performance of Various Filters on Skin Cancer Images," *Procedia Computer Science*, vol. 42, pp. 32–37, Jan. 2014, https://doi.org/10.1016/j.procs.2014.11.030.

[6] H. Hu and G. erard de Haan, "Classification-based hybrid filters for image processing," in *Visual Communications and Image Processing 2006*, Jan. 2006, vol. 6077, pp. 361–370, https://doi.org/10.1117/12.642138.

[7] R. S. Kumar, K. M. Nagaraja, G. D. Chethankumar, B. J. Nandini, and K. R. Chinni, "Properties of Oscillatory Mean Involving Power Exponential Mean and Power Mean," vol. 22, no. 6, pp. 1117–1124, Apr. 2023.

[8] S. M. Sagari, V. P. Malagi, and S. Sasi, "Euri – A Deep Ensemble Architecture For Oral Lesion Segmentation And Detection," *International Journal of Intelligent Systems and Applications in Engineering*, vol. 12, no. 3s, pp. 242–249, 2024.

[9] B. S. Venkataramana, K. M. Nagaraja, R. Sampathkumar, and M. A. Hejib, "The Properties of One Parameter Power Exponential Mean and Its Invariants," vol. 20, no. 7, pp. 1197–1208, May 2021.

[10] H. Wang *et al.*, "Iterative Window Mean Filter: Thwarting Diffusion-Based Adversarial Purification," *IEEE Transactions on Dependable and Secure Computing*, vol. 22, no. 2, pp. 1827–1844, Mar. 2025, https://doi.org/10.1109/TDSC.2024.3472569.

[11] M. Gatcha, F. Messelmi, and S. Saadi, "An Anisotropic Diffusion Adaptive Filter for Image Denoising and Restoration Applied on Satellite Remote Sensing Images: A Case Study," *Engineering, Technology & Applied Science Research*, vol. 12, no. 6, pp. 9715–9719, Dec. 2022, https://doi.org/10.48084/etasr.5363.

[12] S. Bhat, V. Malagi, K. Rangarajan, and R. Babu, "Computer vision based guidance in UAVs: software engineering challenges," *SIGSOFT Softw. Eng. Notes*, vol. 35, no. 6, pp. 1–6, Aug. 2010, https://doi.org/10.1145/1874391.1874399.

[13] L. Rajesh and H. S. Mohan, "Shuffled Shepherd Squirrel Optimization and Fractional LMS Model for In-Network Aggregation in Wireless Sensor Network," *International Journal of Business Data Communications and Networking (IJBDCN)*, vol. 18, no. 1, pp. 1–21, Jan. 2022, https://doi.org/10.4018/IJBDCN.309412.